AIP | Journal of Applied Physics

Boundary layer charge dynamics in ionic liquid-ionic polymer transducers

Jacob D. Davidson and N. C. Goulbourne

Citation: J. Appl. Phys. **109**, 014909 (2011); doi: 10.1063/1.3524189
View online: http://dx.doi.org/10.1063/1.3524189
View Table of Contents: http://jap.aip.org/resource/1/JAPIAU/v109/i1
Published by the AIP Publishing LLC.

Boundary layer charge dynamics in ionic liquid-ionic polymer transducers

Jacob D. Davidson and N. C. Goulbourne[a)]
Department of Aerospace Engineering, University of Michigan, Ann Arbor, Michigan 48109, USA

(Received 21 May 2010; accepted 1 November 2010; published online 7 January 2011)

Ionic polymer transducers (IPTs), also known as ionic polymer-metal composites, are soft sensors and actuators which operate through a coupling of microscale chemical, electrical, and mechanical interactions. The use of an ionic liquid as solvent for an IPT has been shown to dramatically increase transducer lifetime in free-air use, while also allowing for higher applied voltages without electrolysis. In this work, we apply Nernst-Planck/Poisson theory to model charge transport in an ionic liquid IPT by considering a certain fraction of the ionic liquid ions as mobile charge carriers, a phenomenon which is unique to ionic liquid IPTs compared to their water-based counterparts. Numerical simulations are performed using the finite element method to examine how the introduction of another pair of mobile ions affects boundary layer charge dynamics, concentration, and charge density distributions in the electric double layer, and the overall charge transferred and current response of the IPT. Due to interactions with the Nafion ionomer, not all of the ionic liquid ions will function as mobile charge carriers; only a certain fraction will exist as "free" ions. The presence of mobile ionic liquid ions in the transducer will increase the overall charge transferred when a voltage is applied, and cause the current in the transducer to decay more slowly. The additional mobile ions also cause the ionic concentration profiles to exhibit a nonlinear dynamic response, characterized by nonmonotonic ionic concentration profiles in space and time. Although the presence of mobile ionic liquid ions increases the overall amount of charge transferred, this additional charge transfer occurs in a somewhat symmetric manner. Therefore, the additional charge transferred due to the ionic liquid ions does not greatly increase the net bending moment of the transducer; in fact, it is possible that ionic liquid ion movement actually decreases the observed bending response. This suggests that an optimal electromechanical conversion efficiency for bending actuation is achieved by using an ionic liquid where only a relatively small fraction of the ionic liquid ions exist as free ions. Conversely, if it is desired to increase the overall amount of charge transferred, an ionic liquid with a large fraction of free ions should be used. These theoretical considerations are found to be in good qualitative agreement with recent experimental results.
 [doi:10.1063/1.3524189]

I. INTRODUCTION

Ionic polymer transducers (IPTs), also known as ionic polymer-metal composites (IPMCs), are an emerging class of smart materials with applications as soft sensors and actuators. These transducers consist of an ion-exchange membrane (typically Nafion) placed in a certain cation form (such as Li^+ or Na^+), solvated with a polar solvent, and electroded on both sides. When a dc voltage (1–5 V) is applied to the faces of an IPT in a cantilever configuration, the transducer will bend toward the anode as shown in Fig. 1. Conversely, a voltage will be generated by an IPT when a mechanical deformation is imposed. These transduction properties are the result of ion and solvent transport through the thickness of the membrane. Recent work has specifically focused on using ionic liquids in IPTs.[1–9] The environmental and electrochemical stability of an ionic liquid in actuator systems allows for lasting device performance in free-air usage and at higher applied potentials.[10,11]

In order to model actuation and ultimately improve the performance of IPT actuator systems, an accurate description of the charge transport mechanisms is needed. To this end, modeling efforts have focused on a description of ion transport in IPTs by applying the Nernst-Planck/Poisson (NPP) system of equations, and taking the neutralizing countercation to be the only mobile ionic species.[12–17] However, this description is incomplete for newly developed actuator systems which use ionic liquids as solvent. In an ionic liquid IPT, there are three mobile ions: the neutralizing cation and both the anion and cation of the ionic liquid. Specific interactions of the ionic liquid with the ionomer cause not all of the ionic liquids to be "free," i.e., to move under migration with the application of an applied electric field. Recent ex-

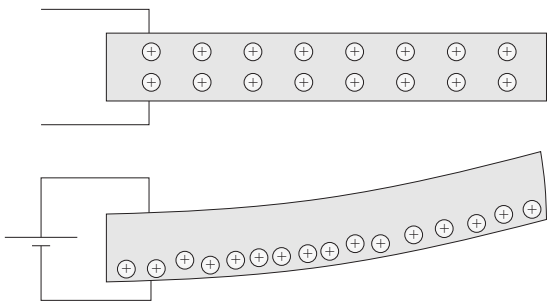

FIG. 1. An IPT will bend toward the anode when a voltage is applied due to cation and solvent movement.

[a)]Electronic mail: ngbourne@umich.edu.

perimental work has examined how the use of different ionic liquids affects actuator performance and charge transport characteristics.[6,7,9] Here, we seek to model the dynamic electrochemical response of an ionic liquid IPT, specifically looking at how the introduction of another pair of mobile ions influences boundary layer charge dynamics, concentration, and charge density distributions in the electric double layer, and the overall charge transferred and current response of the IPT. We consider a certain fraction of the ionic liquid ions as mobile, and demonstrate through numerical simulations how this affects the charging response. As the amount of free ionic liquid ions increases, the ionic concentration profiles are seen to exhibit a nonlinear dynamic response, a feature of electrochemical systems which is discussed by Bazant *et al.*[18] for the case of a binary electrolyte. However, since the IPT has fixed anionic groups, the charge transport problem in the present case becomes highly asymmetric, and it is seen that the nonlinear dynamics are only present when there are free ionic liquid ions in the system. Additionally, the boundary layer charge distributions and the overall amount of charge transferred will change with the addition of mobile ionic liquid ions. We discuss these effects in relation to the actuation and charging response of the transducer, and make suggestions for performance improvements which can be applied to future device development. The paper is organized as follows. In Sec. II A, we describe the ionic liquid IPT system and the assumptions made in order to formulate a model of charge transport. Using NPP theory, the governing system of equations and numerical solution procedure is given in Secs. II B and II C, and the results of the numerical simulations are presented and discussed in Sec. III. Finally, in Sec. V, we summarize and give suggestions for transducer development.

II. MODEL DEVELOPMENT

A. Actuation mechanisms

When a voltage is applied to the faces of an IPT, the mobile ions in the ionomer will move to screen the applied field. The movement of ions causes the formation of thin layers near each electrode that have an excess or a depletion of charge. These layers, referred to as boundary layers, are the "active regions" during actuation. Electrostatic interactions between the ions cause pressures to develop in the boundary layers, and the resulting pressure gradient causes the movement of solvent molecules. The boundary layers will either expand or contract as the solvent molecules move to neutralize the pressure gradient, causing an elastic deformation of the polymer backbone material. Equilibrium will consist of a balance between electrostatic interactions, migration and diffusion potentials, and the resulting elastic stress from boundary layer expansion or contraction. It is found that the cathode boundary layer (CBL) undergoes a larger expansion than the anode boundary layer (ABL), and thus an IPT in a cantilever configuration will bend toward the anode as shown in Fig. 1.

From previous experimental and theoretical studies, it is known that the actuation of an IPT is a direct function of the charge transported when a voltage is applied. Akle *et al.*[19] demonstrated that IPT actuation performance is directly related to capacitance, and thus a direct function of the charge transferred. Onishi *et al.*[20] showed that the overall charge transferred increased with the number of gold platings, but that the optimal number of platings was a midrange value because of the increase in IPT stiffness with number of platings. Asaka and Oguro[21] and Shahinpoor and Kim[22] modeled the deformation of an IPT as the result of solvent flux due to electro-osmosis and changes in osmotic pressure, which varies linearly with the volumetric charge density in the polymer. Porfiri[16] and Chen *et al.*[23] used a similar relationship for electromechanical coupling, saying that the stress in the polymer (and thus the bending moment generated during actuation) is linearly related to the volumetric charge density. Leo *et al.*[24] modeled the stress developed in the polymer during actuation as a sum of linear and quadratic terms of the spatially varying volumetric charge density. This same relation for electromechanical coupling was also used by Wallmersperger *et al.*[13] Nemat-Nasser[12] stated that transported charge causes electrostatic and osmotic pressures to develop in the polymer, which in turn cause solvent flux, boundary layer expansion, and actuation. Our previous work utilizes this approach in modeling ionic liquid IPTs.[8] Other research has focused on equivalent circuit representations of an IPT.[25–30] Farinholt and Leo[29] include a theoretical and experimental analysis of the impedance response of IPTs in the frequency domain.

NPP theory is commonly used to describe ion transport in electrochemical systems (see, for example, Ref. 31), and has been previously applied in analyzing the charge transport characteristics of an IPT. An analytical solution for the equilibrium charge distribution considering a single mobile ionic species in an IPT was given by Nemat-Nasser,[12] and numerical solutions featuring a coupling to the actuation response were obtained by Wallmersperger *et al.*[13,14,17] Porfiri showed that the capacitance of an IPT is a decreasing function of the applied voltage,[15] and incorporated these results into an actuation model to demonstrate the influence of electrode structure on charge transferred and actuation performance.[16] Aureli *et al.*[32] demonstrated how rough electrodes lead to a large increase in capacitance of the IPT, which is best described physically by a large microscopic electrode surface area while keeping the IPT permittivity within reasonable bounds; bounds for IPT permittivity are given by Porfiri.[33] Chen *et al.*[23] used equilibrium numerical solutions of the NPP equations to form a nonlinear circuit model of an IPT. Numerical solutions of the NPP equations in other electrochemical applications have used both the finite difference and finite element methods. Here, we use the finite element method following Lim *et al.*[34] to obtain numerical solutions to the system of governing equations.

Wallmersperger *et al.*[35] used the NPP equations as the basis for a coupled electrochemomechanical model of actuation of ionic polymer gels, and used the finite element method to perform numerical simulations of the response. In Ref. 35, there is a fixed anionic species in the gel, and mobile anions and cations in the gel and surrounding solution. Although multiple mobile ionic species are considered, the boundary conditions and system configuration are signifi-

cantly different than that under present consideration for the ionic liquid IPT, and the transient response in the boundary layers is not a focus of the modeling effort in Ref. 35. A model of multiple mobile ionic species in an ionic liquid IPT currently does not exist in the literature, although several phenomenological discussions regarding this phenomenon in ionic liquid IPTs have recently appeared.[6,7,9]

Our mathematical description of charge transport mechanisms in ionic liquid IPTs is based on the results in Refs. 1 and 36, where ionic liquid IPTs were characterized using small-angle x-ray scattering (SAXS), Fourier transform infrared spectroscopy (FTIR), and nuclear magnetic resonance spectroscopy (NMR). The spectroscopic characterizations led to the conclusion that the countercation is still the main mobile charge carrier in an ionic liquid IPT. FTIR results were used to find the critical uptake of ionic liquid, i.e., the uptake which leads to nearly complete dissociation of the counterions from the fixed anion sites, for membranes in different counterion forms. Alkali metal NMR was performed for ionic liquid-swollen Nafion membranes exchanged with Li^+, Na^+, and Cs^+ counterions as a function of ionic liquid uptake, and the results were used to identify the mobility of the countercation as a function of uptake, using a procedure similar to that done by Komoroski and Mauritz.[37,38] It was found that the mobility of the countercation increases with increasing uptake, reaching a max at high uptake levels, These results were used to describe charge transport mechanisms; the proposed model indicated that the counterions are the primary charge carriers and move through the membrane by "hopping" along ionic liquid anion sites, and that the most important parameter in determining the mobility of the countercation is the amount of ionic liquid present above the critical uptake. Building on these results, we take the countercation to be the main mobile ionic species and consider the presence of an additional pair of mobile ions, which correspond to mobile ionic liquid ions. In this, we aim to identify some of the mechanisms which differentiate ionic liquid IPTs from their water-based counterparts.

B. Transport equations

Ion flux in response to an applied voltage is described by the Nernst-Planck equation

$$J_i = -D_i\left(\frac{\partial c_i}{\partial x} + \frac{z_i c_i F}{RT}\frac{\partial \phi}{\partial x}\right), \tag{1}$$

where J_i is flux, D_i is the diffusion coefficient, c_i is concentration, and z_i is the charge of species i. Symmetry along the length and width of the IPT is presumed to reduce the problem to only the through-thickness direction x, as shown in Fig. 2. Recent results using NMR spectroscopy have shown that Nafion displays a certain degree of diffusion anisotropy, which may result from preferential channel alignment along one of the normal axes created by the manufacturing process.[39] Because of the electrode configuration of an IPT, only the through-thickness direction needs to be considered for actuation, and therefore diffusion anisotropy is not modeled.

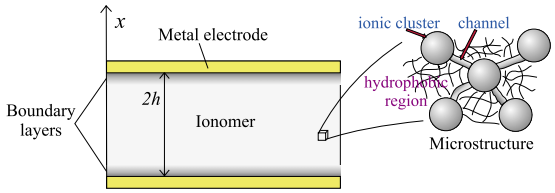

FIG. 2. (Color online) A diagram of the system for modeling ion transport, showing the through-thickness x direction.

Equation (1) is obtained by modeling the ions as point charges, and therefore tends to predict large increases in concentration near the electrodes. At higher applied voltages, as will be demonstrated in Sec. III D, the use of Eq. (1) with three mobile ionic species leads to unrealistic predictions for ionic concentrations. Steric effects due to the large sizes of the ionic liquid ions need to be accounted for to accurately model the ionic liquid ions at higher applied voltages, and this can be done using the modified NPP theory discussed in Refs. 40–42. The use of a modified set of NPP equations applied specifically to model ionic liquids is discussed by Kornyshev[42] and Fedorov and Kornyshev.[43] Applied to a neat ionic liquid, steric effects are accounted for by imposing a maximum concentration for the ionic liquid ions. However, for an IPT system, allowing an ionic liquid ion to reach a concentration higher than its neat solution maximum is correct in a model to a certain extent, since the boundary layers can expand and make room for more ions to fit in. This justifies the use of the classic NPP theory at low applied potentials; however, the range of applicability of Eq. (1) is clearly limited for ionic liquids and the modified theory of Refs. 40–42 needs to be included to model ion transport in ionic liquid IPTs at actuator operating voltages. Nonetheless, a test case considering a low applied voltage using NPP theory can give insight into the movement of multiple mobile ionic species and the resulting charge transport characteristics which are unique to ionic liquid IPTs. We take this approach here. The application of a set of modified NPP equations to model ionic liquid IPTs has been a subject of our recent work.[44]

Modeling the electrodes as blocking electrodes, the initial conditions and boundary conditions are

$$c_i(x,0) = c_i^0, \tag{2a}$$

$$J_i(\pm h,t) = 0, \tag{2b}$$

$$\phi(\pm h,t) = \pm\frac{V_0}{2}. \tag{2c}$$

The transient behavior of the mobile ions is determined by combining Eq. (1) with the expression for conservation of mass

$$\frac{\partial c_i}{\partial t} + \frac{\partial J_i}{\partial x} = 0, \tag{3}$$

and the resulting equation is solved along with the Poisson equation

$$\frac{\partial^2 \phi}{\partial x^2} = -\frac{F}{\bar{\epsilon}} \sum_i z_i c_i, \tag{4}$$

to obtain the transient charge transfer response. Using the boundary conditions [Eq. (2)] along with Eq. (4), it is seen that the potential distribution in the membrane is initially linear, given by $\phi = V_0 x/(2h)$.

In Eq. (4), $\bar{\epsilon}$ is the effective permittivity of the IPT, which is defined using a bulk capacitance measurement to incorporate some effects of the interpenetrating electrodes. It is also approximated that $\bar{\epsilon}$ is constant through the thickness of the polymer, which will likely not hold in the boundary layers due to molecular reorientation. However, as is commonly done in modeling the electric double layer, this effect is ignored and the permittivity is taken to be constant. The definition of $\bar{\epsilon}$ using a bulk capacitance measurement effectively changes the length scale of the problem by increasing the Debye length

$$\lambda = \left(\frac{\bar{\epsilon} RT}{c_0 F^2} \right)^{1/2}, \tag{5}$$

and therefore the size of the boundary layers relative to the total thickness of the polymer, $2h$. With this approximation, predictions for the amount of charge transferred when a voltage is applied become on the order of experimental results. Using a capacitance measurement of 0.05 $\mathrm{mF/cm^2}$ for an ionic liquid IPT (Ref. 2) and a hydrated polymer thickness of 200 μm, a simple parallel plate capacitor model yields a very large effective permittivity, $\bar{\epsilon} = 1.13 \times 10^7 \epsilon_0$. Alternatively, the local effective permittivity can be calculated by considering a mixture of ionic liquid, Nafion, free water, and bound water, which have relative permittivities of 15.1, 3, 78, and ~7.5, respectively.[33,45,46] Hashin-Shtrikman bounds are given in Ref. 33 for the permittivity of water-hydrated Nafion, where a sample with volume fraction of 0.3 (volume solvent/total volume) was said to have a permittivity in the range $6.4 < \bar{\epsilon} < 20$. For the ionic liquid IPT system, the bounds for permittivity will be lower than this, since an ionic liquid has a permittivity much less that of free water. The two definitions lead to vastly different values of the effective permittivity which differ by ~6 orders of magnitude. The parallel plate capacitor approximation leads to a large value since the assumption is made that the IPT behaves as a linear dielectric, i.e., there is a linear drop in potential across the whole membrane and therefore the distance between plates of an equivalent capacitor is equal to the thickness of the membrane. Because of the mobile ions, there will only be a potential drop (at equilibrium) over each thin boundary layer, and therefore an equivalent capacitor for the IPT is better described as two series capacitors, each having a distance between capacitor plates on the order of the Debye length. The thinness of the boundary layers leads to the large capacitance of an IPT. Aureli *et al.*[32] and Porfiri[33] showed that the electrode structure is best represented by specifying the microscopic surface area of the electrode and using a local value for the permittivity calculated from a mixture formula. Although this definition may give more direct information about the electrode structure, it leads to numerical instabilities due to the small relative size of the boundary layers to the thickness of the polymer, λ/h. The definition of $\bar{\epsilon}$ using an approximate capacitance measurement has been shown to yield a good comparison with experimental results,[12,13] and this approach is taken here. Further justification for this choice can be taken from the results of applying the method of matched asymptotic expansions to solve the NPP equations.[15,16,18,41,44] From these results, the total charge transferred is independent of the polymer thickness, but the boundary layer charging characteristics depend on the time scale $\tau_C = \lambda h/D_+$, where D_+ is the diffusion coefficient of the countercation. This time scale depends on both the Debye length and the polymer thickness and will be further discussed in Sec. III B. As long as $\lambda/h \ll 1$ and $c_i(\mathrm{bulk}) \sim c_i(t=0)$ hold, the use of an overly large effective permittivity only changes the time scale for the problem. This means that the large effective permittivity can be used in a numerical analysis to obtain the dominant charge transfer characteristics and will only tend to alter the characteristic time scale associated with the response (to a first order approximation). The nonlinear dynamic response associated with the transient ionic concentration profiles is also slightly affected by this definition; this is discussed in Sec. III B. In Sec. III D, we give an example of when $c_i(\mathrm{bulk}) \sim c_i(t=0)$ does not hold, and the numerical analysis and underlying theory are therefore not applicable.

C. Solution procedure

In this analysis there are three mobile ionic species and one fixed negatively charged species. Unlike a typical binary electrolyte solution, this configuration gives rise to a highly asymmetric charge distribution. A finite element method is used to solve Eqs. (1), (3), and (4), and is implemented following the approach of Lim *et al.*[34] for modeling two mobile ionic species. First, the equations are nondimensionalized (denoted by the tilde accent) using

$$\tilde{\phi} = \phi \frac{F}{RT}, \tag{6a}$$

$$\tilde{c}_i = \frac{c_i}{c_0}, \tag{6b}$$

$$\tilde{x} = \frac{x}{\lambda}, \tag{6c}$$

$$\tilde{t} = \frac{t}{\tau} = \frac{tD_+}{\lambda^2}, \tag{6d}$$

where c_0 is the concentration of the fixed anionic groups and $\tau = \lambda^2/D_+$ is the Debye time, which is defined using the diffusion coefficient of the countercation, D_+. The correct time scale for the charge transport problem is actually the charging time,[18,41] $\tau_C = \lambda h/D_+$, as will be discussed in Sec. III B. However, to obtain numerical solutions, the Debye time τ is used in the mathematical formulation and the results are later renormalized. The equations are now written as

$$\tilde{J}_i = -\tilde{D}_i \left(\frac{\partial \tilde{c}_i}{\partial \tilde{x}} + z_i \tilde{c}_i \frac{\partial \tilde{\phi}}{\partial \tilde{x}} \right), \tag{7a}$$

$$\frac{\partial \tilde{c}_i}{\partial \tilde{t}} + \frac{\partial \tilde{J}_i}{\partial \tilde{x}} = 0, \tag{7b}$$

$$\frac{\partial^2 \tilde{\phi}}{\partial \tilde{x}^2} = -(z_1\tilde{c}_1 + z_2\tilde{c}_2 + z_3\tilde{c}_3 - 1), \tag{7c}$$

where the diffusion coefficients $\tilde{D}_i$ are normalized with respect to the diffusion coefficient of the countercation. The nondimensional form of the initial and boundary conditions is

$$\tilde{c}_i(\tilde{x},0) = \frac{c_i^0}{c_0} = \tilde{c}_i^0, \tag{8a}$$

$$\tilde{J}_i(\pm\tilde{h},\tilde{t}) = 0, \tag{8b}$$

$$\tilde{\phi}(\pm\tilde{h},\tilde{t}) = \pm\frac{F}{RT}\frac{V_0}{2} = \frac{\tilde{V}_0}{2}, \tag{8c}$$

where $\tilde{h}=h/\lambda$ is the nondimensionalized thickness parameter ($2h$ is the thickness of the polymer layer—see Fig. 2).

The charge transferred per unit surface area can be calculated as the integral of the charge density over half of the system, i.e.,

$$\tilde{q} = \frac{q}{\lambda F c_0} = \int_{-\tilde{h}}^{0}\sum_j z_j\tilde{c}_j(\tilde{x})d\tilde{x} = -\int_0^{\tilde{h}}\sum_j z_j\tilde{c}_j(\tilde{x})d\tilde{x}. \tag{9}$$

This expression for charge stored in the boundary layers is only valid when the boundary layer size is much smaller than the polymer thickness, i.e., $\lambda \ll h$. When $\lambda \sim h$ an alternate expression would be required; however, this is never the case for an IPT. Here, also since conservation of charge is enforced by the zero flux boundary condition in Eq. (8b), the integral over either half of the domain can be used to determine charge transferred. The current is the change in charge transferred with respect to time

$$\tilde{i} = i\frac{\lambda}{D_+ F c_0} = \frac{d\tilde{q}}{d\tilde{t}}. \tag{10}$$

These are numerically calculated in the finite element framework by defining the appropriate matrix operators to integrate for charge transferred, and differentiate with respect to time to calculate current, as described in Appendix A. Both the charge transferred and current depend on a sum over all the ionic species, and therefore vary directly with the charge density distribution in the membrane. The transient current in response to an applied voltage is the quantity most readily measured experimentally. Details on the finite element solution procedure are given in Appendix A.

III. NUMERICAL RESULTS

A. Parameter description

The system in consideration is an ionic liquid IPT, a common example of which uses EMI-Tf ionic liquid as solvent and Li^+ as the neutralizing countercation. The ionomer membrane is Nafion 117, which has an equivalent weight of 1100 g and is given a swollen thickness of 200 μm to represent an ionic liquid-swollen membrane in an actuator. The three mobile ions are denoted as +, IL^-, and IL^+ for the countercation, ionic liquid anion, and ionic liquid cation, respectively, and the anionic sulfonate groups of the Nafion membrane are considered fixed. The effective Debye length is defined using a capacitance measurement of 0.05 mF/cm^2 for an ionic liquid IPT,[2] which yields $\lambda = 0.152$ μm.

The concentration of the ionic liquid ions in the polymer is known simply from the uptake. However, unlike in a neat ionic liquid, all of the ions of the ionic liquid will not be available to separate and selectively move toward the electrodes. Due to interactions with the Nafion ionomer, some of the ionic liquid ion pairs will continue to exist as dipoles and quadrupoles even when a voltage is applied. Since the amount of free ionic liquid ions is not known, we allow this parameter to vary in the numerical solutions by defining the ratio

$$\alpha = \frac{c_{IL^+}^0}{c_+^0} = \frac{c_{IL^-}^0}{c_+^0}. \tag{11}$$

In an ionic liquid IPT, there will still be water in the system from an equilibration with room humidity. In Ref. 8, it was determined that the average water uptake for Nafion at an equilibrium with typical room humidity is ~0.155 (volume water/volume dry polymer). This accounts for the estimated water content of ~1 water molecule per sulfonate group still remaining in Nafion after drying in a vacuum at room temperature until equilibrium.[47,48] Water will also exist in the neat ionic liquid, and its presence will generally decrease the viscosity, increase the ionic conductivity, and decrease the electrochemical window of the ionic liquid.[49] Recently, experimental results using *in situ* proton NMR have shown that on the order of one water molecule per ionic liquid cation-anion pair will exist in Nafion swollen with EMI-Tf ionic liquid in addition to the equilibrium water content of the membrane.[50] With these considerations, the number of ionic liquid ion pairs per sulfonate group, n_{IL}, and the number of water molecules per sulfonate group, n_w, are calculated as[8]

$$n_{IL} = \frac{EW}{\rho_B}\left(\frac{w-\bar{w}_w}{V_{IL}+V_w}\right), \tag{12a}$$

$$n_w = \frac{EW}{\rho_B}\left(\frac{\bar{w}_w}{V_w} + \frac{w-\bar{w}_w}{V_{IL}+V_w}\right), \tag{12b}$$

where $w = V_{solvent}/V_{polymer}$ is the solvent uptake, $\bar{w}_w$ is the average water uptake before adding ionic liquid, EW is the equivalent weight and ρ_B is the dry density of the ionomer, and V_w and V_{IL} are the partial molar volumes of water and ionic liquid, respectively. Using $\bar{w}_w = 0.155$, $EW = 1100$ g/mol, $\rho_B = 2.0$ g/cm^3, $V_w = 18$ cm^3/mol, and $V_{IL} = 187.2$ cm^3/mol for EMI-Tf ionic liquid, an ionic liquid IPT with a total solvent uptake of 80 vol % has an ionic liquid uptake of 58 vol % (~40 wt %), or $n_{IL} = 1.7$. This corresponds to the uptakes of the ionic liquid actuators fabricated in Ref. 7. However, as discussed by Li *et al.*,[50] uptakes as high as $n_{IL} = 4.4$ can be achieved by longer periods

of soaking while heating near the glass transition temperature of Nafion. Therefore, for typical ionic liquid IPT actuators, an approximate range for the number of ionic liquid ions per sulfonate group can be established as $1<n_{IL}<4.5$, with most actuators having $n_{IL}\sim 2$.

Since the countercation is expected to still be the main mobile charge carrier, we take α to be small in the numerical calculations. It is likely that the number of free ionic liquid anions and cations is not equal, possibly with more free cations because of the association of counterions with ionic liquid anions, and because some of the counterions may be exchanged with ionic liquid cations via diffusion when the membrane is swollen with ionic liquid. The applied field may also affect the amount of free ionic liquid ions. Free ions only exist when the interaction energy between the ions is overcome by other exchanges of energy. At equilibrium, the probability distribution of the energies of the individual molecules will follow a Boltzmann distribution, and ion pairs with energies greater than a certain threshold will dissociate. The energy required for dissociation of the ionic liquid ion pairs in Nafion will be different from that of a neat ionic liquid due to interactions with the ionomer. This determines the initial amount of free ions. When a voltage is applied, the electric field will act as an applied force which polarizes the ionic liquid ion pairs and causes more pairs to dissociate. In the initial nonequilibrium period as current flows due to ion movement, there will be a nonzero electric field through the thickness of the membrane. At equilibrium, there will be a large electric field in each boundary layer, but the potential in the bulk region outside the boundary layers will be constant. The transient nonequilibrium electric field in the bulk region causes the amount of free ionic liquid ion pairs to increase as the system moves toward equilibrium. The probability of an ion pair being dissociated by the applied electric field varies with the magnitude of the applied field, and thus the rate at which ion pairs in the bulk region become dissociated will decrease exponentially with time. For a larger applied voltage, the field will initially be greater in magnitude and more ion pairs will become dissociated. Therefore, the total amount of free ionic liquid ions will increase with time as the system moves toward equilibrium, and at equilibrium will vary with the magnitude of the applied voltage. However, the extent of this effect is unknown, and in the present analysis we take α to be constant for simplicity.

Due to their large sizes, the ions of the ionic liquid are expected to move more slowly than the small countercations. As a first approximation, the diffusion coefficients of the ionic liquid ions are given an equal value, denoted as

$$\beta=\frac{D_{IL^+}}{D_+}=\frac{D_{IL^-}}{D_+}. \tag{13}$$

Due to interactions with the ionomer and the different sizes of the ions, this is known to not be the case in a real system. Li *et al.*[50] used NMR to measure the diffusion coefficients of the anion and cation of EMI-Tf ionic liquid in Nafion, and the results at room temperature showed an average ratio of $D_{IL^+}/D_{IL^-}=1.5$ (averaged over different ionic liquid uptakes), with this ratio decreasing with uptake. However, again for simplicity, we retain the approximation of equal diffusion coefficients in order to examine the dominant trends in the charge transfer response when mobile ionic liquid ions are present.

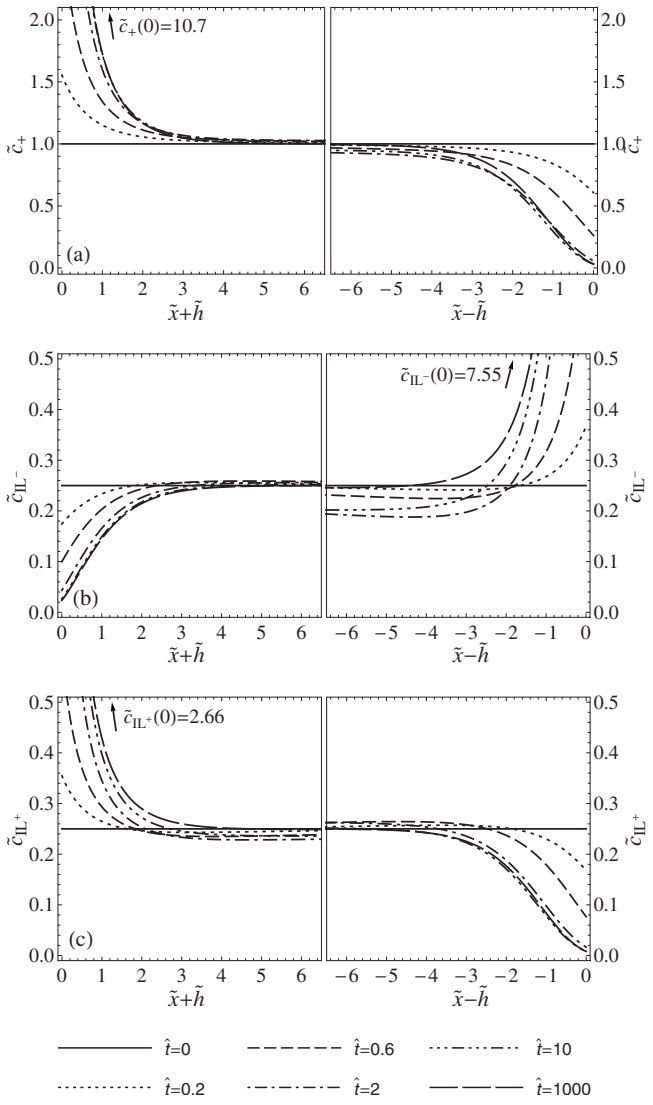

FIG. 3. Transient boundary layer concentration profiles for $V_0=0.15$ V, $\alpha=0.25$, and $\beta=0.1$, showing (a) the countercation, (b) the ionic liquid anion, and (c) the ionic liquid cation.

B. Transient ionic concentration profiles

The finite element method is used to solve the governing equations given in Sec. II C and was implemented in a MATHEMATICA code. To analyze the response, a test case with an applied voltage of $V_0=0.15$ V is considered. This is low compared to typical IPT operating voltages ($\sim$1 V), but we will show in Sec. III D that the use of classic NPP theory at higher applied voltages with 3 mobile ionic species leads to unreasonably large predictions for ionic concentration at the electrodes. Nonetheless, a test case within a valid voltage range can give insight into the mechanisms of ion transport, and these results are shown here.

Figures 3 and 4 show the evolution of the boundary layers when the step voltage $V_0=0.15$ V is applied at $t=0$. Figure 3 shows results for the parameter values $\alpha=0.25$ and $\beta=0.1$, and Fig. 4 for the same relative diffusion coefficient

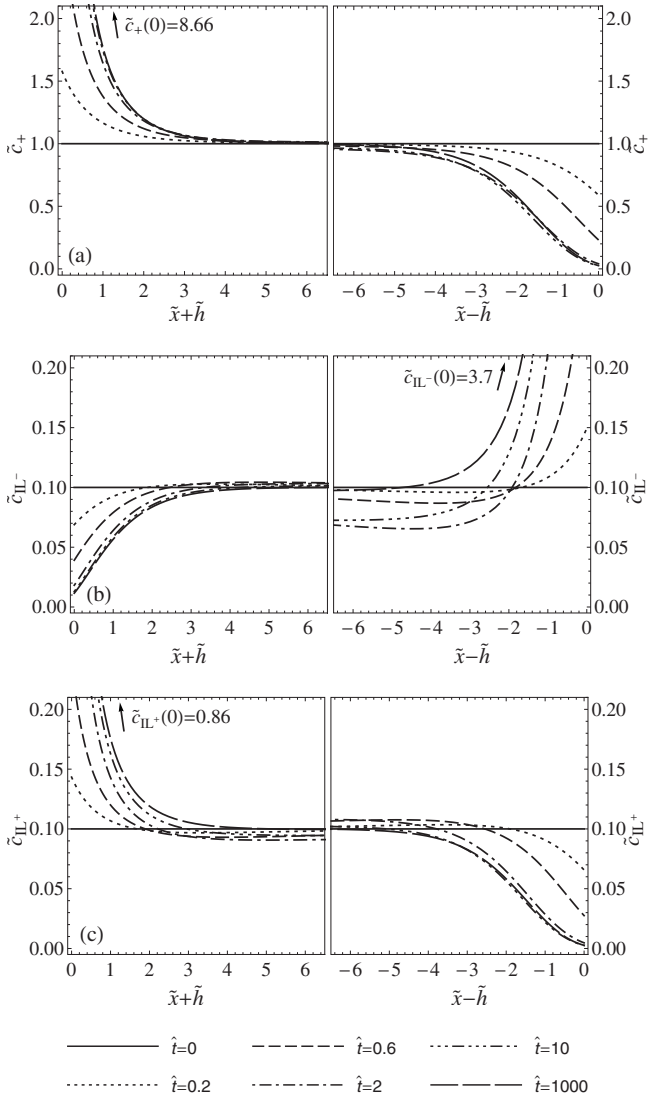

FIG. 4. Transient boundary layer concentration profiles for $V_0=0.15$ V, $\alpha=0.1$, and $\beta=0.1$, showing (a) the countercation, (b) the ionic liquid anion, and (c) the ionic liquid cation.

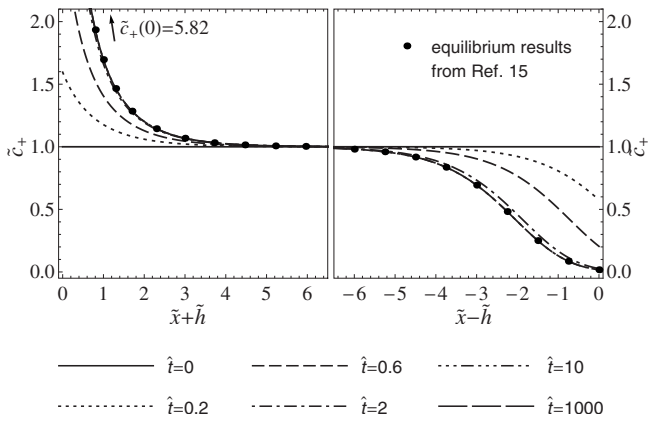

FIG. 5. Transient boundary layer concentration profiles for $V_0=0.15$ V and $\alpha=0$, showing movement of the countercation. The results at equilibrium ($\hat{t}=1000$) are compared to results generated using the solution method in Ref. 15.

but a smaller fraction of free ionic liquid ions, $\alpha=0.1$ and $\beta=0.1$. Recall that α is the fraction of free ionic liquid ions to counterions and β is the relative diffusion coefficient of the ionic liquid ions to the counterion. These parameter values are chosen since it is expected that the countercation is still the main mobile charge carrier and that the ionic liquid ions move slowly compared to the countercation due to their large sizes. To display these results, time is normalized by the charging time scale $\tau_C=\lambda h/D_+$, i.e., time is displayed using $\hat{t}=t/\tau_C$. When the voltage is applied, the two cationic species move toward the negatively charged electrode and the anion moves toward the positively charged electrode. The concentration of each ion is exponentially increasing at these corresponding electrodes, and the maximum concentration at the electrode for $\hat{t}=1000$ is shown on each graph. The concentration of each ion is depleted at the opposite electrode, e.g., the concentration of each cation decreases at the anode compared to its initial state. With multiple mobile ionic species the transient response is nonmonotonic in space and time: at certain points the concentration will decrease and then increase, or vice versa, and the concentration of each ionic liquid ion decreases and then increases going from one electrode to the other. This effect is most noticeable for the ionic liquid anion, shown in Figs. 3(b) and 4(b). The nonlinear dynamic response is discussed by Bazant *et al.*[18] and Kilic *et al.*[41] for the case of a binary electrolyte solution. For a water-based IPT, where $\alpha=0$, the dynamic response is linear (i.e., monotonic) as shown in Fig. 5. The equilibrium ionic concentration profile of the countercation in Fig. 5 is compared to results generated using the matched asymptotic expansion solution procedure in Ref. 15, showing an excellent agreement. This agreement is expected since the basic assumption that must hold for the matched asymptotic solution to be valid is $\lambda/h \ll 1$ (the solution considers the limit as $\lambda/h \to 0$), and for these numerical results we used $\lambda/h=1.52\times10^{-3}$, which is $\ll 1$. Note that in Ref. 15 the results of the matched asymptotic analysis were compared and found to be in excellent agreement with the numerical results in Wallmersperger *et al.*,[14] so the results of our present numerical analysis for $\alpha=0$ are thus consistent with previous numerical solutions of the NPP equations for a single mobile ionic species in IPTs.

In Fig. 4, where $\alpha=\beta=0.1$, we see that even a small amount of mobile ionic liquid ions causes the concentration profiles of all the ions to exhibit some nonlinear dynamics. With $\alpha=0.1$, the countercation is the main mobile charge carrier and only shows a small amount of nonlinear dynamics. In this case, the biggest difference in the response versus a water-based IPT (where $\alpha=0$) is in the ABL, where the presence of a mobile anion now causes there to be a region of increasingly negative charge density near the electrode.

For each parameter set, the time needed for the system to reach equilibrium is much longer than for the case of $\alpha=0$, which is shown in Fig. 5. Even for the case of $\beta=1$ (all ion diffusion coefficients equal) the time needed to reach equilibrium will be much longer than that needed for a water-based IPT due to the nonlinear dynamic response, which introduces an additional diffusive time scale. With multiple mobile ionic species a total of three time scales emerge: the Debye time $\tau=\lambda^2/D_+$, a charging time scale dependent on the Debye length, $\tau_C=\lambda h/D_+$, and a diffusive time scale de-

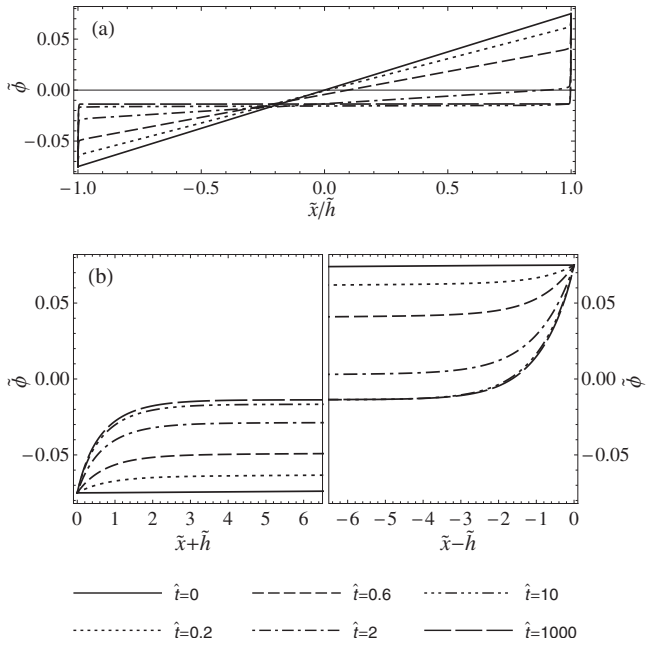

FIG. 6. Transient potential profiles for $V_0=0.15$ V and the parameter values $\alpha=0.25$ and $\beta=0.1$, showing potential (a) across the membrane and (b) zoomed in on the boundary layers.

pendent only on the size of the system, $\tau_D=h^2/D_+$. The Debye time corresponds to the time needed for ions to move into the boundary layers. During charging, the boundary layers will be in a state of quasi-equilibrium with the bulk region, with their composition determined at leading order by the potential drop from the diffuse region to the bulk region (the zeta potential). Defining the zeta potential for each boundary layer to be the difference in potential at the electrode with the potential at the beginning of the bulk region, where charge density is zero, the zeta potential varies with time according to the charging time scale τ_C. The total amount of charge transferred thus depends on τ_C. The additional diffusive timescale τ_D contributes to the response when large amounts of ion adsorption create a temporary local depleted region just outside the boundary layers.[18] This leads to a nonlinear dynamic response, the extent of which depends on the ionic concentrations and applied voltage. Bazant *et al.*[18] discuss this behavior and gives limits for weakly and strongly nonlinear behavior considering a typical binary electrolyte solution. However, these bounds do not apply to an IPT system due to the asymmetric nature of the charge transfer problem. When $\alpha=0$, only linear dynamics are present as shown in Fig. 5. When $\alpha>0$, the nonlinear response becomes visible, as shown in Figs. 3 and 4.

As noted in Ref. 8, the nonmonotonic concentration profiles of the ions are more prevalent when β is small, i.e., when the ionic liquid ions move more slowly than the countercations. Considering the large sizes of the ionic liquid ions compared to the countercation and the experimental observation that ionic liquid IPTs actuate more slowly than water-based IPTs, it is realistic to take β as small. The increased nonlinear dynamic response for small β can be explained by considering the transient potential distribution in the membrane, an example of which is shown in Fig. 6. For $\beta\ll 1$, i.e., the ionic liquid ions move much slower than the counterions, the response can be considered as two problems, each separately in equilibrium with the other: an asymmetric problem for the countercation and a (mostly) antisymmetric problem for the ionic liquid ions. The response for the ionic liquid ions will only be completely antisymmetric in the limit of low applied voltage, since the response defined in this manner depends on the spatially varying potential distribution due to the movement of the countercation, which is antisymmetric at low applied voltages but soon becomes quite asymmetric. For the case of $\beta\ll 1$, it can be approximated that the countercation has reached its equilibrium distribution before the ionic liquid ions start to move into the boundary layers. In this case there will be a large potential gradient near the boundary layers, and zero potential gradient in the bulk region. Ionic liquid ions will move under migration into the boundary layers, causing the formation of a depleted region which will fill in via diffusion according to the diffusive time scale τ_D as the system moves toward equilibrium. Now consider the case of $\beta=1$. As ionic liquid ions move into the boundary layers, a depleted region will still form, but now the countercation will not have reached its equilibrium distribution. There will still be a potential gradient in the bulk region and ionic liquid ions will initially move under diffusion *and* migration to fill in the depleted region. As the potential gradient in the bulk goes to zero, the ionic liquid ions will continue to move under diffusion to fill in the depleted region, but the region will already be somewhat filled in due to the initial "help" from migrative flux via the nonequilibrium bulk potential gradient. Thus, the case of $\beta\ll 1$ displays more nonlinear dynamics in reference to the transient concentration profiles of the ionic liquid ions. Because of the asymmetry of the problem, the countercation concentration profile also shows the most nonlinear dynamic behavior when $\beta\ll 1$.

In examining the nonlinear dynamic response from the numerical results, the use of the effective permittivity $\bar{\epsilon}$ to define a large Debye length should be kept in mind. This definition increases τ_C, making it closer to, although still much less than, τ_D. If $\bar{\epsilon}$ was set to a value corresponding to the local permittivity, τ_C would decrease and it is likely that the results would show more of a nonlinear dynamic response, since τ_C and τ_D would then be farther apart.

C. Potential, charge density, charge transferred, and current

Figure 6 shows the potential distribution with respect to time for the same parameter values used in Fig. 3, $\alpha=0.25$ and $\beta=0.1$. Because of the asymmetry in the concentrations of mobile anions and cations, the potential distribution will be asymmetric. The potential in the bulk region where the charge density is zero will be linear, eventually reaching a constant, nonzero value at equilibrium. This equilibrium bulk potential "offset" is caused by asymmetry and will be largest for the case with the largest asymmetry in mobile ion concentrations, i.e., for a water-based IPT with $\alpha=0$. For an IPT, the nonzero bulk potential at equilibrium is negative and thus tends to decrease the magnitude of the zeta potential in the CBL and increase it in the ABL. Since there are a larger number of mobile cations available to move into the CBL

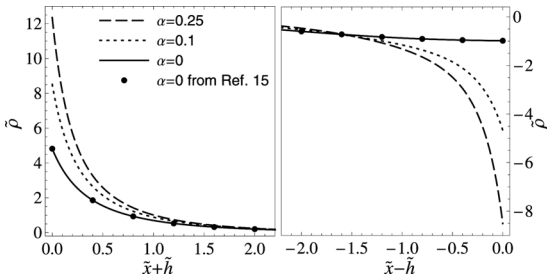

FIG. 7. Equilibrium boundary layer charge density profiles for $V_0=0.15$ V and different values of α. The case of $\alpha=0$ is compared with results generated using the method in Ref. 15.

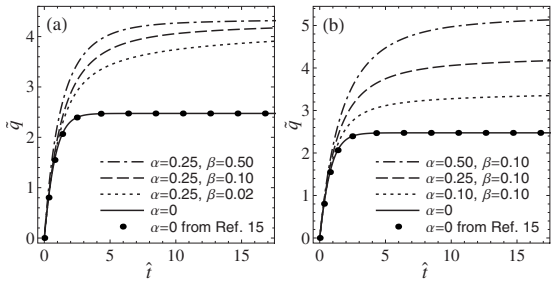

FIG. 8. Charge transferred with respect to time for $V_0=0.15$ V, shown with parameter sets (a) varying β and (b) varying α. The case of $\alpha=0$ is compared with results generated using the method in Ref. 15.

than mobile anions available to move into the ABL, the nonzero bulk potential thus tends to decrease the overall amount of charge transferred. In the boundary layer region nearest the electrodes, Fig. 6(b) shows that the potential follows an exponential distribution.

Figures 3 and 4 showed the nonlinear dynamic response of the individual ionic concentration profiles. The nonmonotonic behavior comes from the presence of an additional diffusive time scale, τ_D. Because of the coupling between the chemical and electrical fields in the NPP equations, diffusive movement will also slightly affect the charge density, which is calculated in nondimensional form as

$$\tilde{\rho}(\tilde{x}) = \frac{\rho}{Fc_0} = \sum_j z_j \tilde{c}_j(\tilde{x}). \tag{14}$$

However, the change in charge density induced by diffusive movement is quite small compared to the magnitudes of charge density in the boundary layers, and the overall boundary layer charging process is dominantly monotonic in terms of charge density. To compare the charge density for an ionic liquid IPT versus a water-based IPT we therefore just compare equilibrium results. Figure 7 shows the equilibrium charge density profiles for an applied voltage of 0.15 V and different amounts of free ionic liquid ions. The relative diffusion coefficient of the ionic liquid ions only affects the charging dynamics, so the equilibrium response is only affected by α. In comparing the ionic liquid IPT charge density distributions ($\alpha>0$) with that of a water-based IPT ($\alpha=0$), the most notable difference is in the ABL which now has an increasingly negative charge density due to the presence of a mobile anion. Additionally, the magnitude of the maximum charge density at both the anode and cathode is larger for larger values of α.

The charge transferred and current with respect to time are shown in Figs. 8 and 9 for different parameter sets of α and β. In Figs. 8(a) and 9(a), the fraction of free ionic liquid ions is held constant and the relative diffusion coefficient of the ionic liquid ions is varied, and in Figs. 8(b) and 9(b) the relative diffusion coefficient of the ionic liquid ions is held constant and the fraction of free ionic liquid ions is varied. For comparison, the result for a water-based IPT, i.e., $\alpha=0$, is also shown on each graph, and compared to results generated using the solution method in Ref. 15. In Fig. 8(a), only the transient response is affected when β is varied. The total amount of charge transferred as $t\to\infty$ is independent of β, but strongly depends on α, as is demonstrated in Fig. 8(b). As α increases, the total amount of charge transferred will increase. When $\beta\ll 1$, the ionic liquid ions move more slowly and thus the maximum charge transferred is reached at later times—this is shown in Fig. 8(a) by the different shapes of the curves. For the water-based IPT represented by $\alpha=0$, the total amount of charge transferred is less than that for the ionic liquid IPT cases, and the equilibrium charge transferred is reached more quickly.

In Fig. 9, the difference between an ionic liquid IPT and a water-based IPT is clearly seen. The initial current response is determined mostly by the quick movement of the counterion. For the water-based IPT represented by $\alpha=0$, the current decay is nearly a neat exponential so it shows as approximately linear when plotted on a log scale. For the ionic liquid IPT, the slower ionic liquid ions cause the current to deviate from neat exponential behavior. This highlights a difference that has been observed experimentally for ionic liquid IPTs: the current decays more slowly than that for a water-based IPT. However, the slower current decay seen in experimental results is likely also due to a difference in ionic mobility of the countercation in an ionic liquid versus water-based IPT. Bennett[1,36] showed that the number of ionic liquid molecules above the critical uptake is the most important parameter in determining the mobility of the countercation. The interpenetrating electrodes also play a large role in determining the transient response; this point will be further discussed in Sec. IV and Appendix B. The slow decay of the current response of the ionic liquid IPT at longer times is determined mainly by the value of β. In Fig. 9(a), it is seen that the current response is initially nearly the same for the different values of β, but becomes different at later times. When β is small, the equilibrium charge transferred is

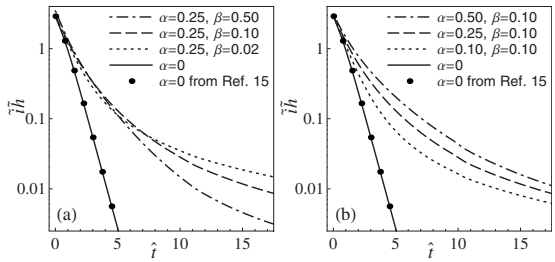

FIG. 9. Current with respect to time for $V_0=0.15$ V, shown with parameter sets (a) varying β and (b) varying α. The case of $\alpha=0$ is compared with results generated using the method in Ref. 15.

reached more slowly, so current does not drop off as fast after the sharp initial drop. However, it should be noted that the change in response for different values of β is only noticeable after the current has already decreased by over an order of magnitude from its initial peak value. In Fig. 9(b), varying α is seen to have a different effect on the current response. As α increases, the overall amount of charge transferred increases, and the slow ionic liquid ions cause the current to drop off more slowly. The change in the response is noticeable at shorter times as α increases, but at long times (past the scale of the graph), the response is nearly identical for the different values of α with fixed β. The slow current decay at long times is due to the nonlinear dynamics and occurs on the order of the diffusive timescale τ_D. The peak current at $\hat{t}=0$ for the cases in Fig. 9 is similar, although it increases slightly for larger values of α and β.

With multiple mobile ionic species, there will be multiple time scales associated with boundary layer charging (e.g., τ_C and τ_C/β). The current decay is therefore better described as stretched instead of simple exponential decay. Because the governing equations are nonlinear, the current decay is actually best described by an infinite sum, but can be well approximated by the sum of a stretched exponential and a slow-decaying exponential to capture the response at long times. Since the nonlinear dynamics contribute to the slow decay at long times, the time scales involved with current decay include τ_C, τ_C/β, τ_D, and τ_D/β.

The current response in Fig. 9 was calculated using Eq. (10), which was nondimensionalized using the Debye time, $\tau=\lambda^2/D_+$. As discussed in Sec. III B, the zeta potential in the boundary layers dominantly varies with the charging time $\tau_C=\lambda h/D_+$, and thus the dominant time scale for the charge transport problem is τ_C. Therefore, calculations for current are displayed in Fig. 9 by computing $\tilde{i}h/\lambda=\tilde{i}\tilde{h}$. With this definition, it becomes apparent that the current through the IPT varies inversely with the polymer thickness, i.e., the magnitude of the current response will be less for an IPT with a thicker polymer membrane. Additionally, Eq. (9) shows that the total charge transferred is independent of the polymer thickness. This follows from the definition of the Debye length and is well known in analyzing the electric double layer.[31]

D. Ionic concentrations at higher applied voltages

As previously mentioned, classic NPP theory is not applicable to describe the ionic liquid IPT system at higher applied voltages. To illustrate, consider the boundary layer concentration profiles shown in Fig. 10 for an ionic liquid IPT system with $\alpha=\beta=0.1$ and an applied voltage of $V_0=1$ V. At equilibrium, the solution predicts that a very large amount of ions accumulate at the electrodes; the maximum calculated concentrations at $\hat{t}=1000$ are $\tilde{c}_+=663$, $\tilde{c}_{\mathrm{IL}^-}=685$, and $\tilde{c}_{\mathrm{IL}^+}=60.2$, which are physically unrealistic, especially for the ionic liquid ions. The case of $\alpha=0$, however, still leads to reasonable results for the ionic concentration of the countercation, with a calculated equilibrium concentration of $\tilde{c}_+=38.7$ at the cathode for 1 V applied (not shown). This demonstrates that NPP theory is reasonable in the application

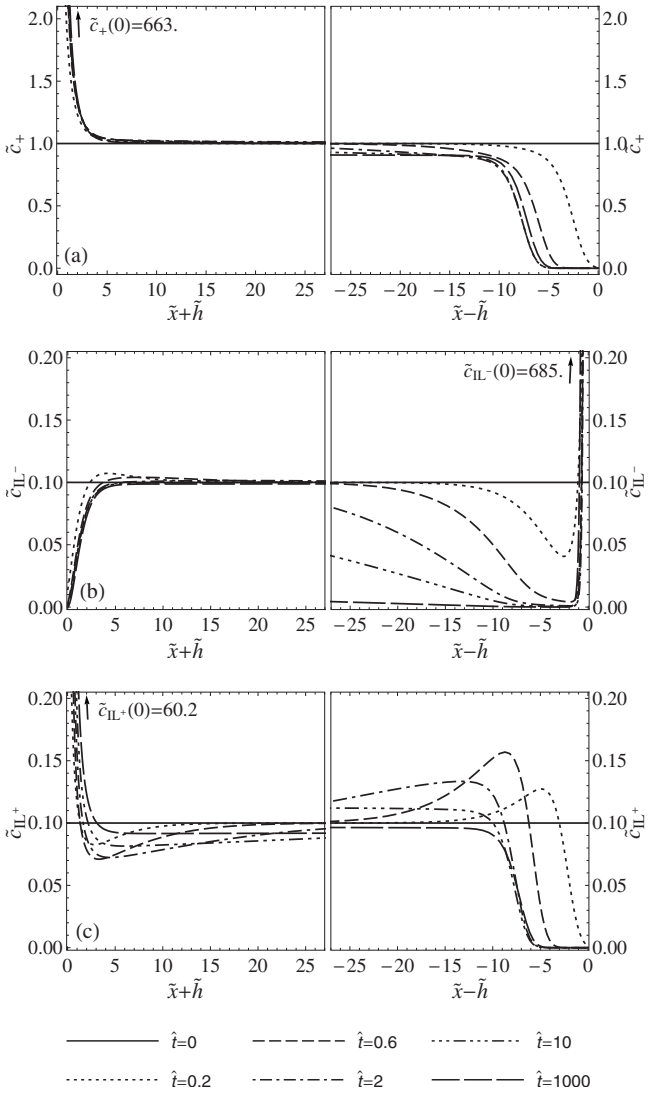

FIG. 10. Transient boundary layer concentration profiles for $V_0=1$ V and $\alpha=\beta=0.10$, showing (a) the countercation, (b) the ionic liquid anion, and (c) the ionic liquid cation.

to IPTs for voltages on the order of 1 V when a single mobile ionic species is considered, but leads to large overpredictions in concentration when considering multiple mobile ionic species, even for small values of α. To model the electrochemical response of the large ionic liquid ions at high applied potentials, the modified Nernst-Planck theory discussed in Refs. 40–42 needs to be used. In Secs. III B and III C, the test cases are shown with an applied voltage of 0.15 V, which is within the range of applicability of NPP theory for the ionic liquid IPT system.

IV. DISCUSSION: EFFECTS OF MULTIPLE MOBILE IONIC SPECIES ON NET CHARGE TRANSFERRED AND ACTUATION RESPONSE

When a voltage is applied to the faces of an IPT, the mobile ions in the polymer move toward the electrodes to form boundary layers. In these layers, electrostatic interactions cause a pressure gradient to form which in turn causes solvent transport, boundary layer expansion, and a macroscopically observable deformation of the entire membrane.

Here, we discuss how these processes are affected by the presence of the additional mobile anion and cation in an ionic liquid IPT, and give recommendations for optimal device performance.

Figure 8 demonstrates that the presence of free ionic liquid ions will tend to increase the net charge transferred in response to an applied voltage. The relationship between charge transferred and α, the ratio of free ionic liquid ions to counterions, also depends strongly on the applied voltage. For small V_0, the total charge transferred will be a linear function of α. As V_0 increases, the relationship becomes exponential using classic NPP theory, since as shown in Sec. III D higher applied voltages lead to large overpredictions in concentration at the electrodes. Generally, if it is desired to increase the total amount of charge transferred, the total amount of free ionic liquid ions should be maximized. This would be the case, for example, to optimize the performance of a solid-state electrochemical supercapacitor.

Although the presence of free ionic liquid ions will tend to increase the total amount of charge transferred, this does not necessarily mean it will increase the actuation response in bending of a transducer. As discussed in Ref. 8, where a micromechanics model is applied to model the actuation of ionic liquid IPTs, the effects of the mobile ionic liquid ions on actuation are from a balance of boundary layer expansion due to the finite size of the ionic liquid ions and boundary layer expansion due to changes in solvent flux caused by the different charge density distribution due to the presence of free ionic liquid ions. Because there are several mechanisms that contribute to the overall response, it is not clear whether mobile ionic liquid ions will tend to increase or decrease the actuation response in terms of displacement of an IPT. Specifically, the mobile anion will contribute to expansion of the ABL, and this expansion will make a contribution to the overall bending moment of the device. The CBL has a higher charge density and will expand by a larger amount, thus making a much larger contribution to the net bending moment than that from ABL expansion; this is why the transducer has an overall bending motion toward the anode. The bending moment created by expansion of the ABL has a sign opposite that of the CBL, and therefore will reduce the net bending moment of the transducer. However, the free ionic liquid ions also cause additional charge to be accumulated in the CBL, and this will cause an increase in the net bending moment that may or may not negate or overcome the negative contribution from ABL expansion. It is possible that even though the ionic liquid IPT will have more charge transferred for a given applied voltage (assuming identical electrode configurations between the ionic liquid and water-based IPTs), ABL expansion will cause the ionic liquid IPT to have less bending tip displacement than the water-based IPT.[51]

Since the mobile anion will have a negative effect on bending actuation, this suggests that the maximum electromechanical conversion efficiency for bending movement of an ionic liquid IPT actuator may occur when α is small. This effect was confirmed qualitatively in Ref. 7, where IPTs with four different ionic liquids were examined experimentally. These authors concluded that the IPTs with EMI-Tf had the highest capacitance but lowest electromechanical conversion efficiency in regards to actuation, and that the IPTs with EMI-BF_4 had the lowest capacitance but highest electromechanical conversion efficiency. From *ab initio* electronic structure calculations using the hybrid B3LYP functional with a 6-31+G^* basis set, it was also found that EMI-Tf had the lowest binding energy while EMI-BF_4 had the highest. Liu *et al.*[7] explained the difference in response by saying that the tightly bound EMI-BF_4 ions form double and triple-ion clusters which move very slowly under the applied field. These results can be explained with our model by taking α to be higher for the EMI-Tf IPT versus the EMI-BF_4 IPT. It should be noted, however, that the transducers in Ref. 7 were likely in proton form (it was not stated whether the counterion was exchanged), and the mechanisms of charge transport for protons versus alkali metal ions in Nafion are known to be different. Protons move through both the Grotthuss mechanism of hopping between water molecules and via diffusion as hydronium ions, with the latter mechanism contributing $\sim$20% to the overall proton mobility in water.[52–55]

It was also found that the different ionic liquid actuator systems all performed similarly in terms of their displacement response, but the total charge transferred for each system was quite different. This was explained in terms of the negative contribution of ABL expansion to the net bending moment discussed above, although it was taken that boundary layer expansion due to movement of the ionic liquid ions occurs solely due to ion size effects. As discussed by Davidson,[8] the effects of multiple mobile ionic species on actuation will be from a balance of both ion size effects and pressure-driven solvent movement due to changes in the charge density distribution. However, it is quite possible that one effect will dominate the other. Liu *et al.*[7] also observed that the actuators reached near the maximum strain long before the maximum amount of charge had been transferred. This effect can be explained in the current model framework by taking $\beta \ll 1$ and assuming that movement of the ionic liquid ions contributes little (or none) to the observed actuation response.

Since there are several unknown factors that could influence these results, including the electrode configuration, fraction of free ionic liquid ions α, relative diffusion coefficient β, and the extent of steric effects in determining the composition of the electric double layer when an ionic liquid is incorporated, a general relation describing the performance of an ionic liquid IPT cannot be given. However, the results here suggest the following performance trends to be true: to increase the overall charge transferred, increase α, and to increase the electromechanical conversion efficiency for bending actuation, decrease α. A decrease in α corresponds to an ionic liquid where less ion pairs are free, and more will tend to stay associated in dipole and quadrupole configurations when a voltage is applied. These interactions depend on the ionic liquid, and on the specific interactions of the ionic liquid with the ionomer. It should also be noted that interactions with the fixed anionic groups of Nafion may cause the ions of the ionic liquid to have very large differences in their transport properties. Specifically, the anion may experience a large barrier to movement through the membrane due to re-

pulsive coulombic interactions with the fixed anion groups, which is expected since Nafion is known and widely used for its permselective properties. However, a large ionic liquid anion may be less influenced by these interactions than a smaller anion like Cl^-, since the charge on the ionic liquid anion will be more delocalized. An equivalent (or better) performance increase in the actuation response compared to decreasing α may be given by using an ionic liquid which has an anion that is relatively immobile compared to the cation when placed in Nafion.

In our numerical solutions, the electrodes were not explicitly treated, and a large effective permittivity was defined to increase the boundary layer size and therefore avoid numerical instabilities. The electrodes will have two notable effects on the performance and charging dynamics of an IPT, besides directly affecting the total amount of charge transferred (the large microscopic area of the electrodes causes an increase in capacitance of 1–4 orders of magnitude[16]): different microscopic surface areas will results in further asymmetries in charge transport characteristics,[16] and the fractal nature will cause the ion adsorption process to exhibit a range of times scales, which is demonstrated experimentally by a stretched-exponential current decay.[32] The influence of the former on the results can be visualized by considering the potential distribution in the membrane, an example of which is shown in Fig. 6. Because the ABL [which is near $\tilde{x}/\tilde{h}=1$ in Fig. 6(a)] will grow as charge accumulates, the total potential drop over the ABL (the ABL zeta potential) will be greater than the CBL zeta potential. Different microscopic surface areas of the electrodes will effectively alter the bulk potential offset and the boundary layer zeta potentials, which, at equilibrium, determine the leading order results in the limit of thin boundary layers for boundary layer composition and charge transferred. As shown by Porfiri,[16] if the microscopic cathode electrode surface area ($\mathcal{S}^-$) is greater than the microscopic anode electrode surface area ($\mathcal{S}^+$), the bulk potential offset will decrease. If $\mathcal{S}^- < \mathcal{S}^+$, the bulk potential offset will increase. This changes the boundary layer concentration profiles, e.g., $\mathcal{S}^- < \mathcal{S}^+$ will cause the magnitude of the CBL zeta potential to increase and therefore its composition will be given by the result for a slightly higher applied voltage, while the composition of the ABL will be given by the result for a slightly lower applied voltage. The fractal-like structure of the interpenetrating electrodes will also affect the charging dynamics; this effect is briefly discussed in Appendix B. A more detailed discussion in regards to interpreting existing experimental data within our current model framework is given in Appendix C.

V. CONCLUSIONS

We examined the dynamic charging characteristics of ionic liquid IPTs by considering the ions of the ionic liquid in addition to the neutralizing countercation as mobile ions. Using NPP theory, numerical solutions describing ionic concentration, charge density, potential, charge transferred, and current were obtained using the finite element method. The distributions of concentration, charge density, and potential were found to be quite asymmetric through the thickness of the membrane, with distinct differences compared to a water-based IPT. The results also reveal that the ionic concentration profiles exhibit a nonlinear dynamic response which is dependent on the relative fraction of free ionic liquid ions α and their relative diffusion coefficient β. Specifically, the concentration profiles depend on both the charging time scale $\tau_C=\lambda h/D_+$ and the diffusive time scale $\tau_D=h^2/D_+$. The current decay in response to an applied step voltage is also affected by both τ_C and τ_D, with the latter describing the slow decay at long times.

The presence of mobile ionic liquid ions causes the ABL to have an increasingly negative charge density near the anode, whereas when $\alpha=0$ the maximum charge density in the ABL will be constant, corresponding to the fixed anionic sulfonate groups of Nafion. This movement of anions into the ABL will reduce the overall bending response of the actuator. As α increases, the total charge transferred increases, but this does not necessarily mean the bending actuation response will increase. This suggests the following trends to optimize device performance: to increase the overall charge transferred, increase α, and to increase the electromechanical conversion efficiency in bending actuation, decrease α.

It was also shown that NPP theory leads to unreasonable predictions for concentrations at the electrodes when the applied potential is increased to ~ 1 V. To extend the results here to IPT operating voltages, a modified Nernst-Planck theory including steric effects needs to be used. However, the numerical solutions here are expected to be within the range of applicability of classic NPP theory, and effectively highlight some of the differences in boundary layer charging characteristics which are unique to ionic liquid IPTs.

APPENDIX A: FINITE ELEMENT SOLUTION PROCEDURE

For the finite element formulation, first the weak form of Eq. (7) is derived by multiplying each equation by a test function, ψ, and integrating over the domain. The Galerkin method is used to define the approximation to the solution for each variable and for the test function

$$\tilde{c}_j \approx N_A \tilde{c}_A^j, \tag{A1a}$$

$$\tilde{\phi} \approx N_A \tilde{\phi}_A, \tag{A1b}$$

$$\psi \approx N_A e_A, \tag{A1c}$$

where N_A are the Hermite shape functions, e_A are arbitrary constants, and summation convention is used over indices in CAPS. It should be noted that since a weak form of Eq. (7) only involves first order derivatives of $\tilde{c}_j$ and $\tilde{\phi}$, linear (Lagrange) basis functions are sufficient in obtaining a solution using the finite element method. In Ref. 34 Hermite basis functions were used in order to apply a Stern layer boundary condition using multipoint constraints. Considering the other approximations made and since we limit the analysis to low applied voltages, Stern layer effects are omitted in the numerical analysis here. Since the additional computational time needed to use the higher order basis functions is not a significant problem for this one-dimensional solu-

tion, the formulation with Hermite basis functions was retained and used to generate numerical solutions. In this formulation, both the variable and its first derivative appear as unknowns. Now, using Eq. (A1), the system of equations is written as

$$\Phi_A = \left[N_A \frac{dN_B}{d\tilde{x}} \tilde{\phi}_B \right]_{-\tilde{h}}^{\tilde{h}} - \int_{-\tilde{h}}^{\tilde{h}} \frac{dN_A}{d\tilde{x}} \frac{dN_B}{d\tilde{x}} \tilde{\phi}_B d\tilde{x} + \int_{-\tilde{h}}^{\tilde{h}} N_A \left[N_B \sum_{j=1}^{3} z_j \tilde{c}_B^j - 1 \right] d\tilde{x} = 0, \tag{A2a}$$

$$\Theta_A^i = \int_{-\tilde{h}}^{\tilde{h}} N_A N_B \frac{d\tilde{c}_B^i}{d\tilde{t}} d\tilde{x} + [N_A \tilde{J}_i]_{-\tilde{h}}^{\tilde{h}} + \int_{-\tilde{h}}^{\tilde{h}} \tilde{D}_i \frac{dN_A}{d\tilde{x}} \left(\frac{dN_B}{d\tilde{x}} \tilde{c}_B^i + z_i N_B \tilde{c}_B^i \frac{dN_K}{d\tilde{x}} \tilde{\phi}_K \right) d\tilde{x} = 0, \tag{A2b}$$

where, again, summation convention is only used over indices in CAPS. Since Hermite shape functions are used, there are four equations for each element for Φ_A and Θ_A^i, and $i = 1-3$ for the three mobile ionic species. There is thus a total of eight degrees of freedom at each node, which translates to a total of 16 degrees of freedom per element. The element equations and nodal variables are assembled as

$$\mathrm{G}^e = \{\Phi_1, \Phi_2, \Theta_1^1, \Theta_2^1, \Theta_1^2, \Theta_2^2, \Theta_1^3, \Theta_2^3, \Phi_3, \Phi_4, \Theta_3^1, \Theta_4^1, \Theta_3^2, \Theta_4^2, \Theta_3^3, \Theta_4^3\}, \tag{A3a}$$

$$\mathrm{q}^e = \{\phi_1, \phi_2, c_1^1, c_2^1, c_1^2, c_2^2, c_1^3, c_2^3, \phi_3, \phi_4, c_3^1, c_4^1, c_3^2, c_4^2, c_3^3, c_4^3\}. \tag{A3b}$$

The global system of equations is assembled to be G, with global variables q, and the system of equations is written in matrix form

$$\mathrm{G(q)} = \mathrm{M\dot{q}} + \mathrm{r(q)} - \mathrm{f} = 0. \tag{A4}$$

The contents of M, r(q), and f are given in Appendix A of Ref. 8. Since the governing equations are nonlinear, Newton-Raphson iteration is performed at each time step to obtain the values for the nodal variables q. Using the backward difference method, the algorithm involves expanding Eq. (A4) in a Taylor series about the current approximation for the solution, $\acute{\mathrm{q}}$, keeping first order terms, and rearranging to get

$$\left[\mathrm{M} + \Delta t \left(\frac{\partial \mathrm{r}}{\partial \mathrm{q}} \right)_{\mathrm{q}=\acute{\mathrm{q}}} \right] \chi(\acute{\mathrm{q}}) = -\mathrm{G}(\acute{\mathrm{q}}), \tag{A5}$$

where χ is the correction to the current approximation for the solution. A method to calculate the tangent matrix $\partial \mathrm{r}/\partial \mathrm{q}$ is outlined in Appendix A of Ref. 8. Equation (A5) is solved and the solution for time $t+1$ is updated to be $\mathrm{q}_{t+1} = \acute{\mathrm{q}} + \chi(\acute{\mathrm{q}})$. The residual for the current approximation to the solution is calculated as

$$\gamma = \frac{1}{n^e} \sum_{j=1}^{m} |G_j(\mathrm{q}_{t+1})|, \tag{A6}$$

where n^e is the number of elements and $m = 8(n^e + 1)$ is the total number of equations. If the residual is within acceptable limits, the solution for q_{t+1} is kept and the program moves to the next time step. If γ is not acceptable, $\acute{\mathrm{q}}$ is set equal to q_{t+1} and the process is repeated until the residual is acceptably small. The convergence criteria used in the numerical solution was $\gamma < 10^{-8}$, and the number of elements for all solution sets was $n^e = 300$. To reach equilibrium, the time-step size was increased after the initial ion movement. This was found to sometimes cause a small numerical error to accumulate such that the residual could not be further reduced, so the program was set to automatically reduce the convergence requirement by a factor of 10 if more than 100 iterations were taken for a given time step.

Since the boundary layers are small compared to the thickness of the membrane, a refined mesh is used which places smaller elements near the electrodes. This is done by using a refinement factor, g, and generating elements with increasing/decreasing sizes proportioned by g^n, where n refers to the nth element with respect to either boundary. A refined mesh is needed at both boundary layers since the concentration in both layers will change appreciably when a voltage is applied, so therefore element sizes are defined to increase from $-\tilde{h} < \tilde{x} < 0$ and decrease from $0 < \tilde{x} < \tilde{h}$. This procedure is defined in Ref. 13.

The charge transferred and current with respect to time are also calculated within the finite element framework. The charge transferred is calculated by defining an integral operator

$$H_A = \int_{-\tilde{h}}^{0} N_A d\tilde{x}, \tag{A7}$$

so that Eq. (9) is evaluated using

$$\tilde{q}_N = \sum_j H_A z_j \tilde{c}_A^j(\tilde{t}_N), \tag{A8}$$

where $\tilde{q}_N$ refers to the charge transferred at time step N. To calculate the current, first define the matrices

$$M_{AB}^{\tilde{t}} = \int_0^{\tilde{t}} L_A L_B d\tilde{t}, \tag{A9a}$$

$$K_{AB}^{\tilde{t}} = \int_0^{\tilde{t}} L_A \frac{dL_B}{d\tilde{t}} d\tilde{t}, \tag{A9b}$$

where L_A are the Lagrange interpolation functions and the interpolation is done over time, not space. Now, the current for each time step is calculated with

$$\tilde{i}_N = (M^{\tilde{t}})_{NA}^{-1} K_{AB}^{\tilde{t}} \tilde{q}_B. \tag{A10}$$

Both the charge transferred and current depend on a sum over the different ionic species, and therefore vary directly with the charge density distribution in the membrane.

APPENDIX B: INFLUENCE OF ELECTRODE STRUCTURE ON CHARGING DYNAMICS

The fractal-like structure of the interpenetrating electrodes will have a large effect on the charging dynamics; this was discussed by Aureli *et al.*[32] in regards to IPT charging characteristics, and has been modeled by other researchers in application to fractal electrode structures in other electrochemical systems (see, for example, Refs. 56–65). The fractal dimension of the electrodes is often related to the exponent associated with constant-phase element behavior in the electrochemical impedance response associated with electric double layer charging. A stretched exponential fit to the current response in relation to the fractal dimension of the electrode surface was first suggested by Halsey and Leibig.[57,58] The physical explanation of this behavior is that the fractal electrodes cause multiple time scales to be associated with the charging response, which, when averaged, are exhibited macroscopically as a stretched exponential decay in current. Sakaguchi and Baba found that porous materials also lead to a stretched exponential response.[66] From the numerical results in Fig. 9, the presence of slow-moving ionic liquid ions cause a current decay which can be approximated as stretched exponential, due to the different time scales of charge transfer associated with the different ions. Because there are three processes in a fully-electroded ionic liquid IPT which may contribute to a stretched exponential response, experimentally determining the extent of multiple mobile ionic species migration is difficult. Our recent work has looked at how the capacitance-voltage relationship of an ionic liquid IPT is affected by the presence of multiple mobile ionic species; this is a measure which could alternatively be used to identify α for different ionic liquid IPTs.[44]

APPENDIX C: COMPARISON WITH EXPERIMENTAL OBSERVATIONS

To compare our results with available experimental data for ionic liquid IPTs, first recall from the discussion in Sec. IV and Appendix B that the model in its current form cannot be directly applied to an ionic liquid IPT because of the effects of the electrodes in determining the macroscopically observable charging response. A comparison with experimental results for the electrochemical characteristics of ionic liquid IPTs is therefore restricted to phenomenological and qualitative discussions; a quantitative comparison is beyond the scope of the model in its present form. The comparisons in this section also highlight some of the difficulties in establishing a consistent description of charge transport mechanisms in ionic liquid IPTs.

Lee and Yoo[6] tested ionic liquid IPTs in Li^+ counterion form with four different ionic liquids that had different anions. It was found that a small anion led to a better response in actuation, i.e., higher tip displacement. The electrical resistance of the different transducers, found from the Nyquist plot, was higher for the ionic liquid transducers with larger anions, i.e., ionic conductivity was higher when a small anion was used. However, the transducers with smaller anions had $>25\%$ greater uptake (by mole percent) of ionic liquid, and all of the transducers were also found to have different water uptakes. From the results in Refs. 1 and 36, the molar uptake of ionic liquid above the critical uptake is the most important parameter in describing ionic conductivity, so the difference in conductivity observed in Ref. 6 cannot be attributed solely to anionic mobility. From a simple equivalent circuit model of an ionic liquid IPT consisting of a resistor and capacitor in series, the resistance (times surface area) is

$$R_{\mathrm{IPT}} = \frac{hRT}{F^2 c_0 D_+}\left(\frac{1}{2} + \alpha\beta\right)^{-1}.$$

The difference in ionic conductivity is best attributed to different values of the counterion diffusion coefficient as well as different values of α and β. Unfortunately, these values cannot be identified without additional experimental investigation, such as using alkali-metal NMR to monitor the peak width and relate this to mobility of the counterion, as was done in Refs. 1 and 36.

Lee and Yoo[6] also saw that the IPTs with smaller anions had a larger current density for a given applied voltage, which was inferred from a cyclic voltammogram taken by sweeping ± 3 V at a rate of 100 mV/s. However, these differences are likely due to the onset of electrochemical redox reactions, as can be seen from the cyclic voltammetry, current discharge response to 3 and 4 V step voltages, and linear sweep voltammetry shown in Ref. 6. Therefore, an association of current density and discharge rates with free ionic liquid ion content and relative ionic mobility cannot be made without incorporating redox reactions into the model. It should also be noted that water will still exist in the ionic liquid IPT from an equilibrium with room humidity,[8,50] and this water may be electrolyzed above 1.2 V, although the observed onset voltage of this reaction will be dependent on the catalytic nature of the electrode materials. Therefore, an investigation regarding ionic mobilities and free ionic liquid ion content should reasonably be kept to <1.2 V if redox reactions are to be ignored. Lee and Yoo[6] also compare the amounts of charge transferred after 5 s for the different actuators in response to 3 and 4 V step voltages, but, again, ionic mobility and free ionic liquid ion content cannot be inferred from this without incorporating redox reactions into the model and accounting for the steady-state current.

In Ref. 7, the actuation and charging response of ionic liquid IPTs with four different ionic liquids was experimentally examined. As discussed in Sec. IV, these experimental results are in excellent qualitative agreement with our proposed model. However, since the tests were done on fully-electroded IPTs, it is difficult to infer values of τ_C, α, and β from the transient charging response. To demonstrate, we fit both simple and stretched exponential models to data for the transient charge transferred obtained for three different IL IPTs from Ref. 7 (shown in Fig. 11), and used these fits to obtain the characteristic charging time τ_C. The simple exponential model was used to obtain charging times in Ref. 7, and has the form $q_{\mathrm{simple}} = q_{\mathrm{total}}[1 - \exp(-t/\tau_C)]$. The stretched exponential model accounts for fractal-like electrode structure and steady state current, and was obtained by integrating Eq. 57 of Ref. 32 to obtain

$$q_{\mathrm{str}} = (i_a - i_{ss})\frac{\tau_C}{\eta}\left[\Gamma\left(\frac{1}{\eta}\right) - \Gamma\left(\frac{1}{\eta}, \left(\frac{t}{\tau_C}\right)^{\eta}\right)\right] + i_{ss}t, \qquad \text{(C1)}$$

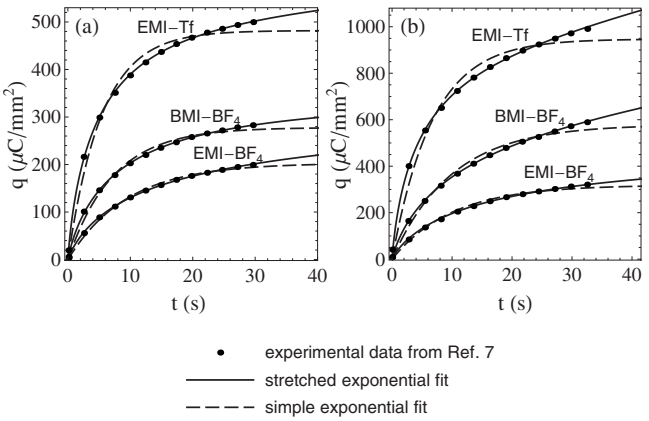

FIG. 11. Experimental data from Ref. 7 for charge transferred with respect to time for different ionic liquid IPTs in response to (a) 2 V and (b) 3 V step voltages, fit using both simple and stretched exponential models.

where i_{ss} is the steady state current, $i_a - i_{ss}$ is the initial current, η is the stretching exponent, which is related to electrode structure ($\eta=1$ is neat exponential behavior), $\Gamma(z) = \int_0^\infty t^{z-1}e^{-t}dt$ is the gamma function, and $\Gamma(z,a) = \int_a^\infty t^{z-1}e^{-t}dt$ is the incomplete gamma function. The stretched exponential looks to be a better fit to the data, especially with the inclusion of the steady state current. All of the stretched exponential fits had $0.45 < \eta < 0.5$, indicating that the electrodes played a large role in determining the transient response.

The charging times are quite different for the two fits; in Fig. 11(a), the simple exponential fit yields $\tau_C = 5.44$, 7.22, 9.48 s for EMI-Tf, BMI-BF_4, EMI-BF_4, while the stretched exponential fit yields 0.87, 1.88, 2.28 s. The determination of the charging time in this manner is thus heavily dependent on the assumptions made in the physical model. These values can also be compared to the expected value for τ_C, calculated as $\tau_C = \lambda h / D_+$. Using Eq. (5) with $c_0 = 1154$ mol/m^3, which corresponds to the 40 wt. % EMI-Tf IPTs in Ref. 7, $2D_+ = D_{IL^-}(40\text{ wt. \%}) + D_{IL^+}(40\text{ wt. \%})$, where $D_{IL^-}(40\text{ wt. \%}) = 4.66 \times 10^{-12}$ m^2/s and $D_{IL^+}(40\text{ wt. \%}) = 7.57 \times 10^{-12}$ m^2/s were calculated by interpolating the data for the room temperature diffusion coefficients of EMI^+ and Tf^- in Nafion as a function of uptake from Ref. 50 (this was done with 50 μm thick Nafion NRE-212, while the transducers in Ref. 7 were made with 25 μm NRE-211, but these should have the same transport properties since both are dispersion cast), and $h = 37$ μm to correspond to the transducer thickness in Ref. 7, the charging time is calculated to be $\tau_C \sim 0.87$ ms using $\bar{\epsilon} = 10\epsilon_0$. Since the diffusion coefficient of the ionic liquid ions is expected to be smaller than the countercation (or of protons), this should be an overestimate of the charging time, but the calculation using a local value of $\bar{\epsilon}$ yields a charging time 3 orders of magnitude lower than that calculated by fitting Eq. (C1), and nearly 4 orders of magnitude lower than that calculated by using the simple exponential fit.

This poor agreement is likely a combination of several effects, including possible electrochemical redox reactions, the electrode structure, the breakdown of NPP theory at higher applied voltages, as demonstrated in Sec. III D, and the influence of steric effects in determining the structure of the electric double layer. To isolate these differences, tests at low voltages should first be performed; this was done by Aureli *et al.*,[32] where a voltage of 10 mV was applied and the charging time was calculated using a stretched exponential fit. In Ref. 32, τ_C was found to vary in the range of 1–20 ms, which is in much better agreement with theoretical predictions than the charging times obtained from the fits in Fig. 11. A similar test applied to ionic liquid IPTs could reveal the charging dynamics associated with different ionic liquids as compared to using water as solvent. Additionally, from the considerations in Appendix B it would be ideal to first test un-electroded samples. With this comparison, it is expected that the ionic liquid would cause more of a stretched exponential current response versus a water-based transducer, as shown in Fig. 9, and the difference in response could possibly be used to identify α and β for different ionic liquids.

[1] M. D. Bennett, Electromechanical transduction in ionic liquid-swollen Nafion membranes, Ph.D. thesis, Virginia Tech, 2005.
[2] M. D. Bennett and D. J. Leo, Sens. Actuators, A **115**, 79 (2004).
[3] B. J. Akle, M. D. Bennett, and D. J. Leo, Sens. Actuators, A **126**, 173 (2006).
[4] J. Wang, C. Xu, M. Taya, and Y. Kuga, Smart Mater. Struct. **16**, S214 (2007).
[5] K. Kikuchi and S. Tsuchitani, J. Appl. Phys. **106**, 053519 (2009).
[6] J. Lee and Y. Yoo, Sens. Actuators B **137**, 539 (2009).
[7] S. Liu, W. Liu, Y. Liu, J. Lin, X. Zhou, M. J. Janik, R. H. Colby, and Q. Zhang, Polym. Int. **59**, 321 (2010).
[8] J. D. Davidson, Actuation and charge transport modeling of ionic liquid-ionic polymer transducers, M.S. thesis, Virginia Tech, 2010.
[9] Y. Liu, S. Liu, J. Lin, D. Wang, V. Jain, R. Montazami, J. Heflin, J. Li, L. Madsen, and Q. Zhang, Appl. Phys. Lett. **96**, 223503 (2010).
[10] M. Armand, F. Endres, D. R. MacFarlane, H. Ohno, and B. Scrosati, Nature Mater **8**, 621 (2009).
[11] W. Lu, A. G. Fadeev, B. Qi, E. Smela, B. R. Mattes, J. Ding, G. M. Spinks, J. Mazurkiewicz, D. Zhou, G. G. Wallace, D. R. MacFarlane, S. A. Forsyth, and M. Forsyth, Science **297**, 983 (2002).
[12] S. Nemat-Nasser, J. Appl. Phys. **92**, 2899 (2002).
[13] T. Wallmersperger, D. J. Leo, and C. S. Kothera, J. Appl. Phys. **101**, 024912 (2007).
[14] T. Wallmersperger, B. J. Akle, D. J. Leo, and B. Krplin, Compos. Sci. Technol. **68**, 1173 (2008).
[15] M. Porfiri, J. Appl. Phys. **104**, 104915 (2008).
[16] M. Porfiri, Phys. Rev. E **79**, 041503 (2009).
[17] T. Wallmersperger, A. Horstmann, B. Kroplin, and D. J. Leo, J. Intell. Mater. Syst. Struct. **20**, 741 (2009).
[18] M. Z. Bazant, K. Thornton, and A. Ajdari, Phys. Rev. E **70**, 021506 (2004).
[19] B. J. Akle, D. J. Leo, M. A. Hickner, and J. E. McGrath, J. Mater. Sci. **40**, 3715 (2005).
[20] K. Onishi, S. Sewa, K. Asaka, N. Fujiwara, and K. Oguro, Electrochim. Acta **46**, 737 (2001).
[21] K. Asaka and K. Oguro, J. Electroanal. Chem. **480**, 186 (2000).
[22] M. Shahinpoor and K. J. Kim, Smart Mater. Struct. **13**, 1362 (2004).
[23] Z. Chen, D. R. Hedgepeth, and X. Tan, Smart Mater. Struct. **18**, 055008 (2009).
[24] D. J. Leo, K. Farinholt, T. Wallmersperger, and Y. Bar-Cohen, *Smart Structures and Materials 2005: Electroactive Polymer Actuators and Devices (EAPAD)* (SPIE, San Diego, CA, USA, 2005), pp. 170–181.
[25] K. M. Newbury and D. J. Leo, J. Intell. Mater. Syst. Struct. **14**, 333 (2003).
[26] J. W. Paquette, K. J. Kim, J. Nam, and Y. S. Tak, J. Intell. Mater. Syst. Struct. **14**, 633 (2003).
[27] P. J. Branco and J. A. Dente, Smart Mater. Struct. **15**, 378 (2006).
[28] C. Bonomo, L. Fortuna, P. Giannone, S. Graziani, and S. Strazzeri, Smart Mater. Struct. **16**, 1 (2007).
[29] K. M. Farinholt and D. J. Leo, J. Appl. Phys. **104**, 014512 (2008).
[30] A. Punning, U. Johanson, M. Anton, A. Aabloo, and M. Kruusmaa, J. Intell. Mater. Syst. Struct. **20**, 1711 (2009).
[31] A. J. Bard and L. R. Faulkner, *Electrochemical Methods: Fundamentals*

and Applications, 2nd ed. (Wiley, New York, 2000).
[32]M. Aureli, W. Lin, and M. Porfiri, J. Appl. Phys. **105**, 104911 (2009).
[33]M. Porfiri, Smart Mater. Struct. **18**, 015016 (2009).
[34]J. Lim, J. Whitcomb, J. Boyd, and J. Varghese, J. Colloid Interface Sci. **305**, 159 (2007).
[35]T. Wallmersperger, B. Krplin, and R. W. Glch, Mech. Mater. **36**, 411 (2004).
[36]M. D. Bennett, D. J. Leo, G. L. Wilkes, F. L. Beyer, and T. W. Pechar, Polymer **47**, 6782 (2006).
[37]R. A. Komoroski and K. A. Mauritz, Perfluorinated Ionomer Membranes **180**, 113 (1982).
[38]R. A. Komoroski and K. A. Mauritz, J. Am. Chem. Soc. **100**, 7487 (1978).
[39]J. Li, K. G. Wilmsmeyer, and L. A. Madsen, Macromolecules **42**, 255 (2009).
[40]I. Borukhov, D. Andelman, and H. Orland, Phys. Rev. Lett. **79**, 435 (1997).
[41]M. S. Kilic, M. Z. Bazant, and A. Ajdari, Phys. Rev. E **75**, 021503 (2007).
[42]A. A. Kornyshev, J. Phys. Chem. B **111**, 5545 (2007).
[43]M. V. Fedorov and A. A. Kornyshev, Electrochim. Acta **53**, 6835 (2008).
[44]J. D. Davidson and N. C. Goulbourne, in *Electroactive Polymer Actuators and Devices (EAPAD) 2*, edited by Y. Bar-Cohen (SPIE, San Diego, CA, 2010), Vol. 7642, pp. 76421L–14.
[45]H. Weingärtner, Z. Phys. Chem. **220**, 1395 (2006).
[46]I. Danielewicz-Ferchmin, J. Phys. Chem. **99**, 5658 (1995).
[47]N. J. Bunce, S. J. Sondheimer, and C. A. Fyfe, Macromolecules **19**, 333 (1986).
[48]T. A. Zawodzinski, M. Neeman, L. O. Sillerud, and S. Gottesfeld, J. Phys. Chem. **95**, 6040 (1991).
[49]P. Hapiot and C. Lagrost, Chem. Rev. **108**, 2238 (2008).
[50]J. Li, K. G. Wilmsmeyer, J. Hou, and L. A. Madsen, Soft Matter **5**, 2596 (2009).
[51]However, the ionic liquid IPT may have more extensional displacement in the thickness direction, due to the additional expansion of the ABL. Thickness-mode IPT actuators are described and discussed in Refs. 67 and 68.
[52]P. Choi, N. Jalani, and R. Datta, J. Electrochem. Soc. **152**, E123 (2005).
[53]M. Eikerling, A. Kornyshev, and E. Spohr, Fuel Cells **1**, 15 (2008).
[54]A. A. Kornyshev and E. Spohr, *Device and Materials Modeling in PEM Fuel Cells* (Springer, New York, 2009), Vol. 113, pp. 349–363.
[55]K. Kreuer, S. J. Paddison, E. Spohr, and M. Schuster, Chem. Rev. **104**, 4637 (2004).
[56]Y. Feldman, E. Polygalov, I. Ermolina, Y. Polevaya, and B. Tsentsiper, Meas. Sci. Technol. **12**, 1355 (2001).
[57]T. C. Halsey and M. Leibig, Phys. Rev. A **43**, 7087 (1991).
[58]T. C. Halsey and M. Leibig, Ann. Phys. **219**, 109 (1992).
[59]R. Kant and S. K. Rangarajan, J. Electroanal. Chem. **552**, 141 (2003).
[60]E. K. Lenzi, L. R. Evangelista, and G. Barbero, J. Phys. Chem. B **113**, 11371 (2009).
[61]T. Pajkossy and L. Nyikos, Phys. Rev. B **42**, 709 (1990).
[62]H. Sakaguchi and R. Baba, Phys. Rev. E **75**, 051502 (2007).
[63]H. Sanabria, Phys. Rev. E **74**, 051505 (2006).
[64]B. Sapoval, *Fractals and Disordered Systems*, 2nd ed., edited by A. Bunde and S. Havlin, (Springer-Verlag, Berlin, 1996), p. 232261.
[65]T. Pajkossy, J. Electroanal. Chem. **364**, 111 (1994).
[66]H. Sakaguchi and R. Baba, Phys. Rev. E **76**, 011501 (2007).
[67]B. J. Akle, Characterization and modeling of the ionomer-conductor interface in ionic polymer transducers, Ph.D. thesis, Virginia Tech, 2005.
[68]B. J. Akle and D. J. Leo, Smart Mater. Struct. **16**, 1348 (2007).